Influence of the interelectrode distance on the production of nanoparticles by means of atmospheric pressure inert gas DC glow discharge

Influence of the inter-electrode distance on the production of nanoparticles by means of atmospheric pressure inert gas dc glow discharge

2014 J. Phys. D: Appl. Phys. 47 415201

(http://iopscience.iop.org/0022-3727/47/41/415201)

IOP Publishing Journal of Physics D: Applied Physics
J. Phys. D: Appl. Phys. **47** (2014) 415201 (12pp) doi:10.1088/0022-3727/47/41/415201

Influence of the inter-electrode distance on the production of nanoparticles by means of atmospheric pressure inert gas dc glow discharge

Esther Hontañón[1], Jose María Palomares[2], Xiaoai Guo[3], Richard Engeln[2], Hermann Nirschl[3] and Frank Einar Kruis[1]

[1] Institute for Technology of Nanostructures (NST) and Center for Nanointegration Duisburg-Essen (CENIDE), University of Duisburg-Essen, Bismarckstr. 81, 47057 Duisburg, Germany
[2] Faculty of Applied Physics, Eindhoven University of Technology, PO Box 513, 5600 MB Eindhoven, The Netherlands
[3] Institute for Mechanical Process Engineering and Mechanics (MVM), Karlsruhe Institute of Technology (KIT), Straße am Forum 8, 76131 Karlsruhe, Germany

E-mail: esther.hontanon@uni-due.de

Received 11 April 2014, revised 15 July 2014
Accepted for publication 11 August 2014
Published 10 September 2014

Abstract

This work is aimed at investigating the influence of the inter-electrode spacing on the production rate and size of nanoparticles generated by evaporating a cathode on an atmospheric pressure dc glow discharge. Experiments are conducted in the configuration of two vertically aligned cylindrical electrodes in upward coaxial flow with copper as a consumable cathode and nitrogen as a carrier gas. A constant current of 0.5 A is delivered to the electrodes and the inter-electrode distance spanned from 0.5 to 10 mm. Continuous stable nanoparticle production is attained by optimal coaxial flow convection cooling of the cathode. Both the particle production rate and the primary particle size increase with the inter-electrode spacing up to nearly 5 mm and strongly decrease with an increasing inter-electrode distance beyond 5 mm. Production rates in the range of 1 mg h^{-1} of very small nanoparticles (<10 nm) are attained by a micro glow discharge (<1 mm); while glow discharges of intermediate sizes (<5 mm) result in production rates of up to 10 mg h^{-1} and primary particles of sizes between 10 and 20 nm. No correlation is found between the measured spatially averaged plasma parameters and nanoparticle production. Since the latter is largely determined by the properties of the cathode surface, spatially resolved spectrometric measurements are needed to discern between the positive column and the cathode region of the glow discharge plasma.

Keywords: glow discharge, interelectrode distance, nanoparticles, particle production rate, primary particle size

(Some figures may appear in colour only in the online journal)

1. Introduction

Electrical discharges in gases at atmospheric pressure have been increasingly gaining attention for cost and energy effectiveness, and sustainable scaling up of nanoparticle mass production. The most common arrangement is that of two electrodes separated by a gap and a gas stream flowing through the gap either in cross- or coaxial-flow configurations. Ongoing efforts are aimed at attaining long-term continuous stable nanoparticle yields of up to a few grams per hour and per electrode pair with controllable particle size and, then, arbitrarily increasing nanoparticle production by operating multiple electrode pairs in parallel [1]. It has been found that two types of electrical discharges, namely spark discharge

and arc discharge, are most suitable for that aim. A newly developed electrical circuit enables the reach of spark frequencies of up to 20 kHz, resulting in production rates higher by a factor of 10^2–10^3 than those achieved by using low frequency spark discharge (<1 kHz), while keeping the primary particle size below 10 nm [2]. Also, the latest advancements in transferred arc nanoparticle synthesis allow for achieving production rates of a few grams per hour with adjustable primary particle size, in general, above 50 nm [3, 4]. The direct current (dc) power supplies needed to drive spark and arc discharges relevant to nanoparticle production differ largely from each other in technical characteristics and price. High voltage (>1 kV) low current (<0.1 A) power supplies are used to ignite and sustain pulsed sparks whose market price is in the order of a few thousands of euros. Arc discharge demands power supplies capable to deliver high currents (>10 A) at low voltages (<30 V) and also high voltage peaks (>1 kV) to start up the arc. Power supplies used in commercial welding devices meet both requirements and are also affordable, with prices well below one thousand euros. Glow discharges build the bridge between transient spark discharge and continuous arc discharge, as it can be attained with currents of typically a few hundred of milliamperes, sustained by voltages of a few hundreds of volts. Atmospheric pressure dc glow discharges are currently disregarded for enhancing nanoparticle production because electronic and temperature instabilities inherent to this type of discharge make them evolve into an arc discharge [5, 6]. Therefore, so far no effort has been made to develop suitable powers supplies to drive glow discharge for that specific application, and the commercially available ones are rather expensive (>10 000 euros).

Nanoparticles of copper were synthesized by an atmospheric pressure nitrogen dc glow discharge in a previous work [7]. This showed that by optimal setup design and choice of process conditions it is feasible to attain stable production of nanoparticles over a wide range of values of the electrical power delivered to the inter-electrode gap. Also, the particle production rate and particle size scaled up with the electrical power. Then, the power spanned from 30 to 200 W by increasing the current (0.3–1 A) with no change or minor reduction in the discharge voltage (300–200 V). The influence of the inter-electrode distance on the production rate and size of nanoparticles produced by an atmospheric pressure dc glow discharge is investigated in this work. At a given current and gas flow rate, the voltage necessary to sustain the glow discharge between two electrodes increases with the inter-electrode spacing and, thus, the power delivered to the gap increases too. Then, the inter-electrode distance is seen as a suitable parameter to control nanoparticle production by means of glow discharge. The arrangement used here is that of two vertically aligned cylindrical electrodes in upward coaxial flow. Experiments are conducted at a constant current of 0.5 A with a consumable electrode of copper and nitrogen as the carrier gas. The production rate and the size distribution of the copper nanoparticles are measured and the light emitted from the glow discharge plasma analysed in dependence of the inter-electrode distance. The lack of spatially resolved information of the plasma renders it difficult to correlate nanoparticle production and size with relevant plasma parameters like the temperature of the gas in the cathode region. Finally, cathode spot patterns evidence different cathode erosion modes resulting in particles of different size scales.

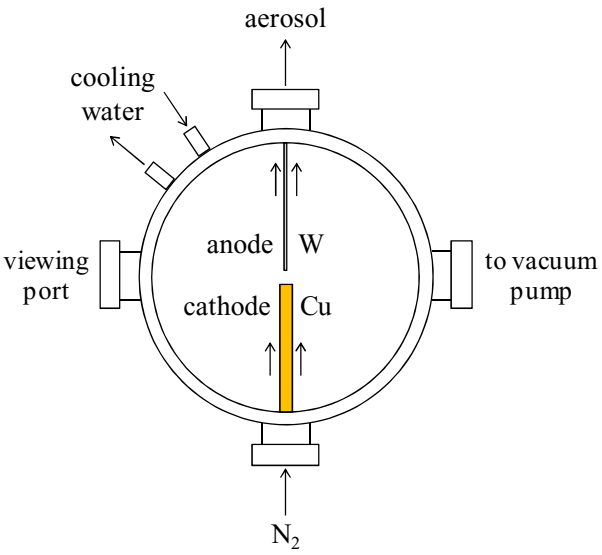

Figure 1. Layout of the setup showing the water cooled chamber, the main ports and the electrode and gas flow arrangement.

2. Experimental

The setup used in this work is described elsewhere [7]. It consists of a vacuum-tight double wall cylindrical chamber with four ports which allow for insertion and set the position of the electrodes within the chamber, to inject the carrier gas and to extract the aerosol from the chamber, as well as to observe the electrical discharge and to monitor the light emitted from the plasma. The electrodes are vertically aligned and a gas stream flows coaxially around in an upward direction, as sketched in figure 1. The electrodes are a tungsten rod (∅1.6 mm, 99.95%, Goodfellow Cambridge Ltd., UK), a copper rod (∅9.5 mm, 99.9%, Goodfellow GmbH, Germany) and the carrier gas is nitrogen (99.999%, Air Liquids GmbH, Germany). The position of the tungsten rod is fixed, whereas the position of the copper rod is adjustable, by means of a linear motor (L2018S0604-T3.5 × 1, Nanotec Electronic GmbH, Germany) controlled by a microstepping driver (5 μm/step, SMCI33, Nanotec Electronic). The discharge is driven by a positive high voltage capacitor charger (CCR10-P-7500, Technix, France) with an adjustable output voltage (⩽10 kV) and current (⩽1.5 A) connected in parallel with a capacitor bank (30 pF) and the inter-electrode gap. The CCR is a current generator; a resonant power supply [8] designed to provide a constant dc current when operated with a capacitive load. The tungsten rod (anode) is connected to the positive voltage output of the CCR and the copper rod (cathode) is connected to ground.

The time averaged discharge voltage between the electrodes is monitored by means of a digital voltmeter

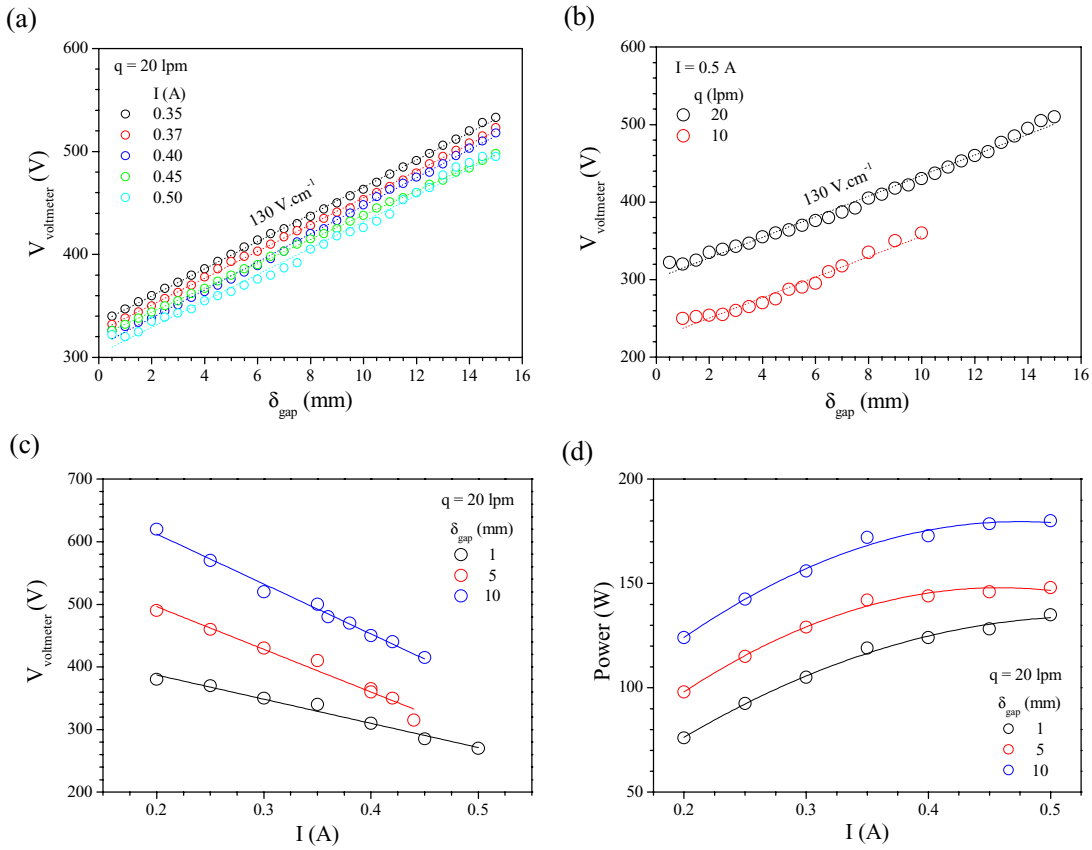

Figure 2. Atmospheric pressure dc glow discharge between a tungsten rod (∅1.6 mm) and a copper rod (∅9.5 mm) in upward coaxial nitrogen flow. Discharge voltage versus gap length in (*a*) experiments at a gas flow rate of 20 lpm and currents in the interval of 0.35 to 0.5 A, and (*b*) experiments at a current of 0.5 A and gas flow rates of 10 lpm (hot cathode) and 20 lpm (cold cathode). Discharge (*c*) voltage and (*d*) power versus current in experiments at a gas flow rate of 20 lpm and gap lengths of 1, 5 and 10 mm.

(Fluke 287). The spectrum of the light emitted from the plasma is recorded by using a spectrometer (AvaSpec 2048-4-DT, Avantes BV, The Netherlands). An unfocused optical fiber is used to collect (90° with respect to the electrode axis) the light from the plasma and nearby electrode rods and, hence, the spectra are neither spatial nor time resolved. The particle size distribution of the copper aerosols is measured by means of a scanning mobility particle sizer (SMPS 3081, TSI Inc., USA). In addition, copper particles are sampled and collected onto PTFE filters (11842-50-N, Sartorius GA, Germany) for gravimetric determination of the particle production rate. Afterwards, the filters are washed and the particles analysed by using transmission electron microscopy (TEM).

3. Parametric investigation

Two sets of preliminary measurements are accomplished with the aim to determine values of the current and the gas flow rate meaningful to nanoparticle production. This is needed for further investigating the influence of the inter-electrode distance on nanoparticle production which is the goal of this work.

3.1. Discharge voltage

The variation of the discharge voltage with the current and the gas flow rate is primarily assessed. In the experiments the current or the gas flow rate are fixed and the gap length is increased stepwise. The time averaged voltage drop along the inter-electrode gap is monitored by using a digital voltmeter. Figures 2(*a*) and (*b*) show the results that correspond to two series of measurements. In one series the nitrogen flow rate is 20 lpm and the current varies from 0.35 to 0.5 A; in the other series the current is 0.5 A and the gas flow rates are 10 and 20 lpm. In all the experiments the discharge voltage varies linearly with the gap length, with a slope of about 130 V cm^{-1}, also referred to as the electric field strength [9–11]. This value is comparable to the values of the electric field strength reported by Arkhipenko *et al* [9] for atmospheric pressure nitrogen glow discharge between tungsten and copper electrodes at currents similar to the ones used here. Significantly lower particle production is found in the experiment at a gas flow rate of 20 lpm with respect to the experiment at a gas flow rate of 10 lpm, suggesting the cathode temperature is higher in the experiment at a lower flow rate (hot cathode). In figure 2(*b*) the discharge voltage is 70–80 V less in the experiment with the hot cathode, which is consistent with the results of Simonchik *et al* [12]. These authors reported a decrease in the discharge voltage of more than 100 V due to cathode heating in atmospheric pressure nitrogen glow discharge. It is noticed that the electric field strength (130 V cm^{-1}) is similar in the experiments at the two gas flow rates, as also observed by Arkhipenko *et al* [13] for an atmospheric pressure helium glow discharge with cooled and

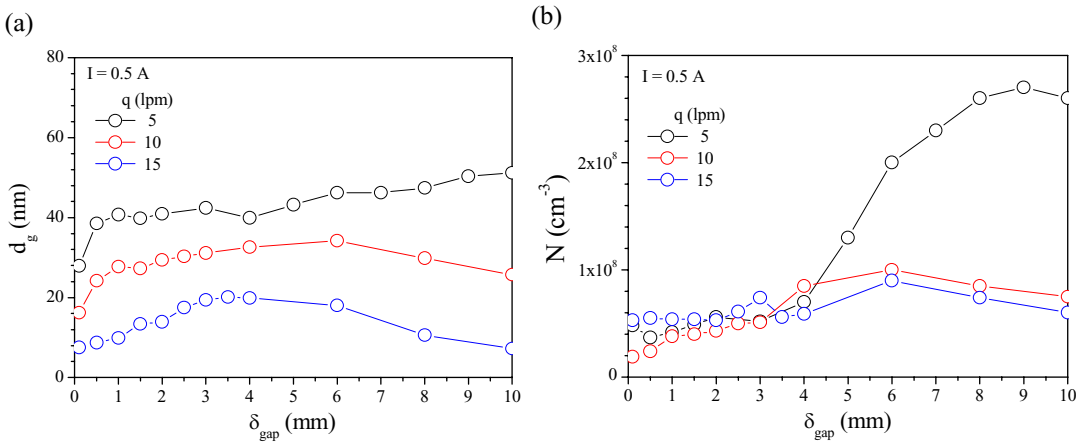

Figure 3. Atmospheric pressure dc glow discharge (0.5 A) between a tungsten rod (∅1.6 mm) and a copper rod (∅9.5 mm) in upward coaxial nitrogen flow. Parameters of the particle size distribution (SMPS) of the copper aerosols versus gap length: (*a*) geometric mean diameter, (*b*) particle number concentration.

Table 1. Process parameters (nitrogen flow rate q, gap length δ_{gap}, discharge voltage $V_{voltmeter}$ and electrical power P); mass production rate $\dot{m}$ and parameters (geometric mean diameter d_g, geometric standard deviation σ_g and particle number concentration N) of the copper particles produced by atmospheric pressure dc glow discharge (0.5 A) between a tungsten rod (∅1.6 mm) and a copper rod (∅9.5 mm) in upward coaxial nitrogen flow.

Filter	q (lpm)	δ_{gap} (mm)	$V_{voltmeter}$ (V)	P (W)	$\dot{m}$ (mg h^{-1})	d_g (nm)	σ_g	N (cm^{-3})	TEM analysis
F1	5	2	300	150	1.2	10.0	1.55	8.3×10^7	—
F2	5	4	250	125	10.7	29.4	1.97	8.3×10^7	Figure 7(*e*)
F3	5	6	260	130	34.0	58.2	1.80	4.9×10^7	—
F4	10	1	250	125	1.1	8.3	1.59	8.0×10^7	Figure 7(*a*)
F5	10	2.5	255	127.5	5.7	14.3	1.95	5.8×10^7	Figure 7(*b*)
F6	10	3	260	130	8.3	18.5	2.01	6.2×10^7	Figure 7(*c*)
F7	10	4.5	275	137.5	11.2	25.6	1.71	6.3×10^7	—
F8	10	7	317	158.5	4.2	21.4	1.73	8.3×10^7	Figure 7(*d*)

uncooled cathodes. The voltage–current characteristic of the glow discharge is measured too. Figures 2(*c*) and (*d*) show the results that correspond to a gas flow rate of 20 lpm and three different gap lengths. As can be seen, the voltage–current curves are descending, whereas the power–current curves are ascending. Similar V–I and P–I trends have been reported for atmospheric pressure normal glow discharges in nitrogen and air by other authors [9, 10, 14, 15].

3.2. Particle size distribution

Next, the particle size distribution of the copper aerosols is measured by means of the SMPS. The production of nanoparticles rises with the glow current as reported in [7]. Almost no particles are detected for currents below 0.35 A. The values of the geometric mean diameter d_g and the particle number concentration N of the copper aerosols produced at a current of 0.5 A are displayed in figure 3. It can be seen that d_g decreases with increasing gas flow rate while N does not vary much with this parameter; except for the experiments at a flow rate of 5 lpm (the reason for this behaviour is given in section 4.1). The SMPS measures the size distribution of the copper particles at the sampling point downstream of the aerosol generator (agglomerates) but it does not measure either the particle production rate or the size of the original particles formed by vapour nucleation in the gap (primary particles).

Figure 2 shows that, at a given current, the discharge voltage and, hence, the electrical power delivered to the gap, increase with increasing inter-electrode distance. The electrical power is obtained as the product of the current (0.5 A) and the discharge voltage. In figure 2(*b*), at a current of 0.5 A and a gas flow rate of 10 lpm, the power rises from 125 to 180 W by enlarging the gap from 1 to 10 mm. The variation of the production rate and the size of the copper particles with the inter-electrode spacing are then investigated. To that aim, experiments are conducted at a current of 0.5 A and gas flow rates of 5 l and 10 lpm. The results are presented and discussed in the following sections.

4. Results

Table 1 summarizes the values of the process parameters in the experiments at a current of 0.5 A, together with the production rate and the parameters of the size distribution of the copper particles. The gap length is adjusted before starting any experiment. The position of the tungsten rod is fixed and the copper rod is lifted up until it touches the tungsten rod (zero gap length). Then, the copper rod is moved down to a certain position whose distance to the tungsten rod determines the gap length δ_{gap} and, then, the discharge is ignited. After ignition, the inter-electrode distance changes due to thermal dilatation

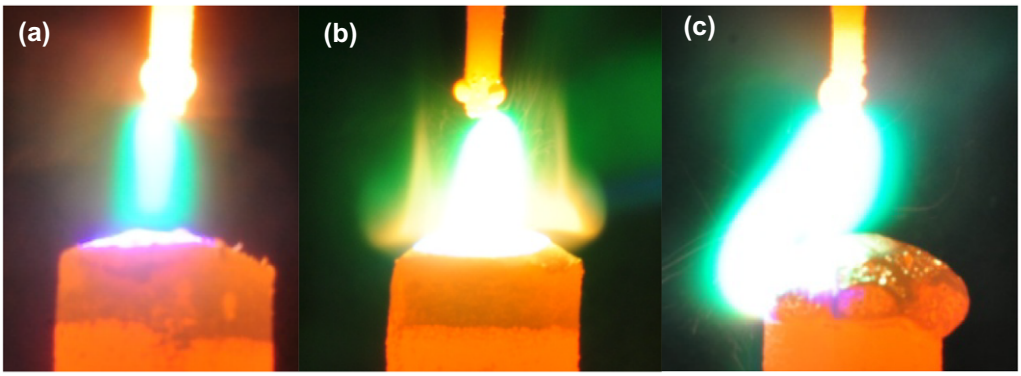

Figure 4. Atmospheric pressure dc glow discharge (0.5 A) between a tungsten rod (∅1.6 mm) and a copper rod (∅9.5 mm) in upward coaxial nitrogen flow (5 lpm) and a gap length of 6 mm. The photographs correspond to (*a*) the beginning of the experiment and 11/2 h later, when a temperature excursion occurs resulting in (*b*) melting of cathode surface and sudden increase in copper release followed by (*c*) melting of cathode top end and cavity formation by ejection of molten copper.

of the anode (see section 4.4) and cathode erosion by the discharge and, hence, does not stay equal to the gap length set before the ignition. Aerosol samples are collected onto filters and the filters weighed before and after particle collection. Then, the particle production rate is calculated from the mass of particles collected onto the filters, the duration of particle collection and the flow rate of the aerosol passing through the filter. The values of the geometric mean diameter, geometric standard deviation and particle number concentration in table 1 are obtained by averaging over a large number (>10) of particle size distributions measured (SMPS) simultaneously to particle filter collection.

4.1. Cathode cooling

Firstly, a series of experiments are conducted at a current of 0.5 A, a gas flow rate of 5 lpm and gap lengths of 2, 4 and 6 mm. Particle collection initiates when the aerosol particle distribution is stable in time, about 30 min after starting the experiments. Then, copper particles are collected onto filters for time periods of 3 h, 1 h and 1/2 h in the experiments with gap lengths of 2 mm (F1), 4 mm (F2) and 6 mm (F3), respectively; and the experiments continue running afterwards. The first glow discharge remains quite stable for the entire duration of the experiment (7 h), while the other two discharges destabilize after about 31/2 h and 11/2 h, respectively. Figure 4 displays the glow discharge at three different time instants in the experiment with a gap length of 6 mm: (*a*) early in the experiment, (*b*) at the time that the discharge becomes unstable and (*c*) a few minutes later. The instabilities appear as a sudden increase of the cathode temperature and the release of copper increases abruptly. This is visually observed by the dense plume of copper rising from the whole surface of the cathode in figure 4(*b*). Afterwards, the top end of the copper rod melts; then, the glow discharge starts moving along the periphery of the cathode, volatilizing and ejecting molten copper into the inter-electrode region and forming cavities, as shown in figure 4(*c*). Clearly the entire surface of the cathode exceeds the melting point of copper (1358 K) in the experiment with a gap length of 6 mm. Then, the structure of the discharge changes and also it becomes highly luminous. It looks much like an arc, although the time averaged voltage and current values correspond to those of a glow discharge. Then, the flow rate of nitrogen is enhanced to 10 lpm to improve cathode cooling and a new series of experiments is accomplished by increasing the gap length from 1 to 10 mm, with a total duration of about 8 h. Copper particles are collected onto filters in experiments with gap lengths of 1 mm (F4), 2.5 mm (F5), 3 mm (F6), 4.5 mm (F7) and 7 mm (F8) for 1 h. No temperature excursion occurs in the experiments at a gas flow rate of 10 lpm. It is observed in figures 5(*a*) and (*b*) that copper removed from the cathode deposits on the periphery of the anode; this effect diminishes with increasing gap length (see section 4.4). The characteristic zones of the glow discharge are recognized in the inter-electrode gap in figures 5(*d*)–(*f*), from bottom to top: a tiny and wide bright region in the vicinity of the cathode surface (negative glow), the Faraday dark space and a narrow and elongated bright region (positive column). Copper vapour is identified by the green colour.

4.2. Nanoparticle production rate and size distribution

The results in table 1 indicate that the particle production rate $\dot{m}$ increases with the interelectrode distance up to a gap length of nearly 6 mm. Typically, microglow discharges (<1 mm) lead to particle production rates in the order of 1 mg h^{-1} and larger glow discharges (1–5 mm) result in particle production rates varying from 1 to 10 mg h^{-1} at a gas flow rate of 10 lpm. The last value of $\dot{m}$ in table 1 (F8) corresponds to a gap length of 7 mm beyond which the mass production rate rapidly diminishes with increasing δ_{gap}. The time needed to collect a meaningful amount of nanoparticles onto the filter ($\geqslant$1 mg) becomes then too long (>8 h), so that no data are provided for larger gaps. The SMPS measurements confirm the variation of the mass production rate with the inter-electrode distance found by gravimetric analysis. The particle size distributions of the copper aerosols generated in the experiments at a gas flow rate of 10 lpm are plotted in figure 6(*a*). Very small nanoparticles (mobility equivalent diameter $d_p < 10$ nm) are produced by microglow discharge. The fraction of such small nanoparticles in the aerosol decreases and the fraction of nanoparticles larger

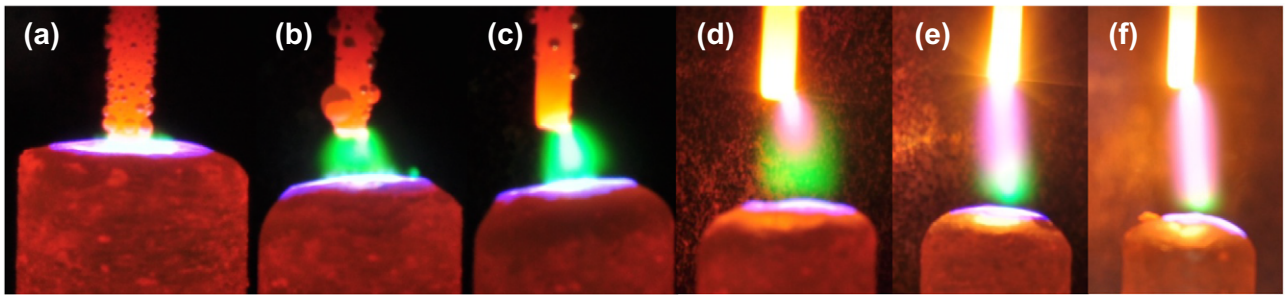

Figure 5. Photographs of atmospheric pressure dc glow discharge (0.5 A) between a tungsten rod (∅1.6 mm) and a copper rod (∅9.5 mm) in upward coaxial nitrogen flow (10 lpm) and gap lengths of (*a*) 1 mm, (*b*) 3 mm, (*c*) 4.5 mm, (*d*) 6.5 mm, (*e*) 8 mm and (*f*) 10 mm.

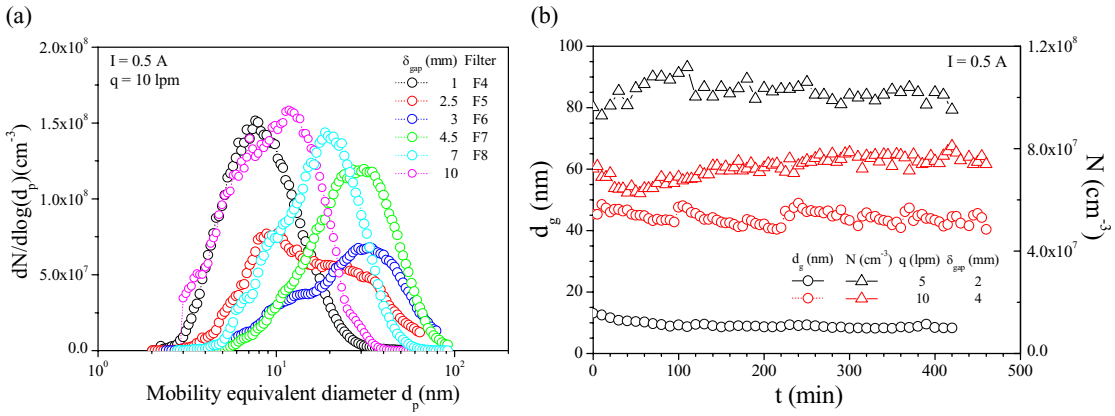

Figure 6. Atmospheric pressure dc glow discharge (0.5 A) between a tungsten rod (∅1.6 mm) and a copper rod (∅9.5 mm) in upward coaxial nitrogen flow. (*a*) Size distribution (SMPS) of copper nanoparticles produced in experiments at a gas flow rate of 10 lpm and the indicated gap lengths; the correspondence with the particle filter samples in table 1 is shown. (*b*) Time evolution of the geometric mean diameter (circles) and the particle number concentration (triangles) of copper nanoparticles produced in experiments at the specified gas flow rates and gap lengths.

than 10 nm increases strongly with increasing gap length. Highly polydisperse particles of sizes spanning from 10 to 100 nm are obtained with gap lengths ranging from 3 to 6 mm. Finally, the size distribution of the copper particles shifts towards smaller particle sizes with increasing inter-electrode distance for gaps larger than 6 mm, consistently with the decreasing production rate. Figure 6(*b*) shows the time evolution of d_g and N in two long duration experiments (7–8 h). The size distribution of the copper particles remains acceptably stable over time. The oscillations observed in d_g are attributed to changes in the position and the temperature at the point that the glow discharge strikes the cathode surface.

The copper particles collected onto the filters are analysed by TEM in order to gain insight into the size, shape, and agglomeration/aggregation state of the primary particles in the aerosol. Figure 7 shows TEM micrographs of the copper particles collected onto filters. Figures 7(*a*)–(*d*) correspond to filters F4, F5, F6 and F8, and figure 7(*e*) corresponds to filter F2. Nanoclusters of a few nanometers in size are mostly observed in figure 7(*a*), as produced by glow discharge in the experiment with a gap length of 1 mm. The fraction of nanoclusters in the aerosol diminishes while the fraction of nanoparticles of sizes between 10 and 20 nm increases with increasing length of the glow discharge, as inferred from figures 7(*b*) and (*c*) corresponding to experiments with gap lengths of 2.5 mm and 3 mm, respectively. The particles in figure 7(*d*) correspond to the experiment with a gap length of 7 mm, and they look much like the nanoclusters in figure 7(*a*). It is noticed that the high population of particles of mobility equivalent diameters d_p larger than 20 nm observed in the aerosol particle size distributions in figure 6(*a*) are not found in the samples, thereby indicating that such large particles are likely agglomerates of smaller primary particles. Finally, the TEM micrograph in figure 7(*e*) corresponds to the nanoparticles produced in the experiment at a gas flow rate of 5 lpm and a gap length of 4 mm. They are spherical and slightly bigger than the nanoparticles in figure 7(*c*) ($\delta_{gap} = 3$ mm). Nanoclusters and nanoparticles show random shapes, are highly aggregated and not very sintered in figures 7(*a*)–(*d*). Nanoparticles form by diffusive and electrostatic agglomeration of nanoclusters in the aerosol phase; whereas particle aggregation occurs mostly in the filter. The temperature history of the aerosol along the path from the plasma region to the filter also plays an important role. High temperatures promote nanocluster coalescence, sintering and compaction of the nanoparticles which then adopt a spherical form, like the spherules in figure 7(*e*).

Gravimetric and TEM analyses of filter samples reveal that, for given current and gap distance, higher production rates and larger primary particles are attained in the experiments at a gas flow rate of 5 lpm, with respect to those at a gas flow

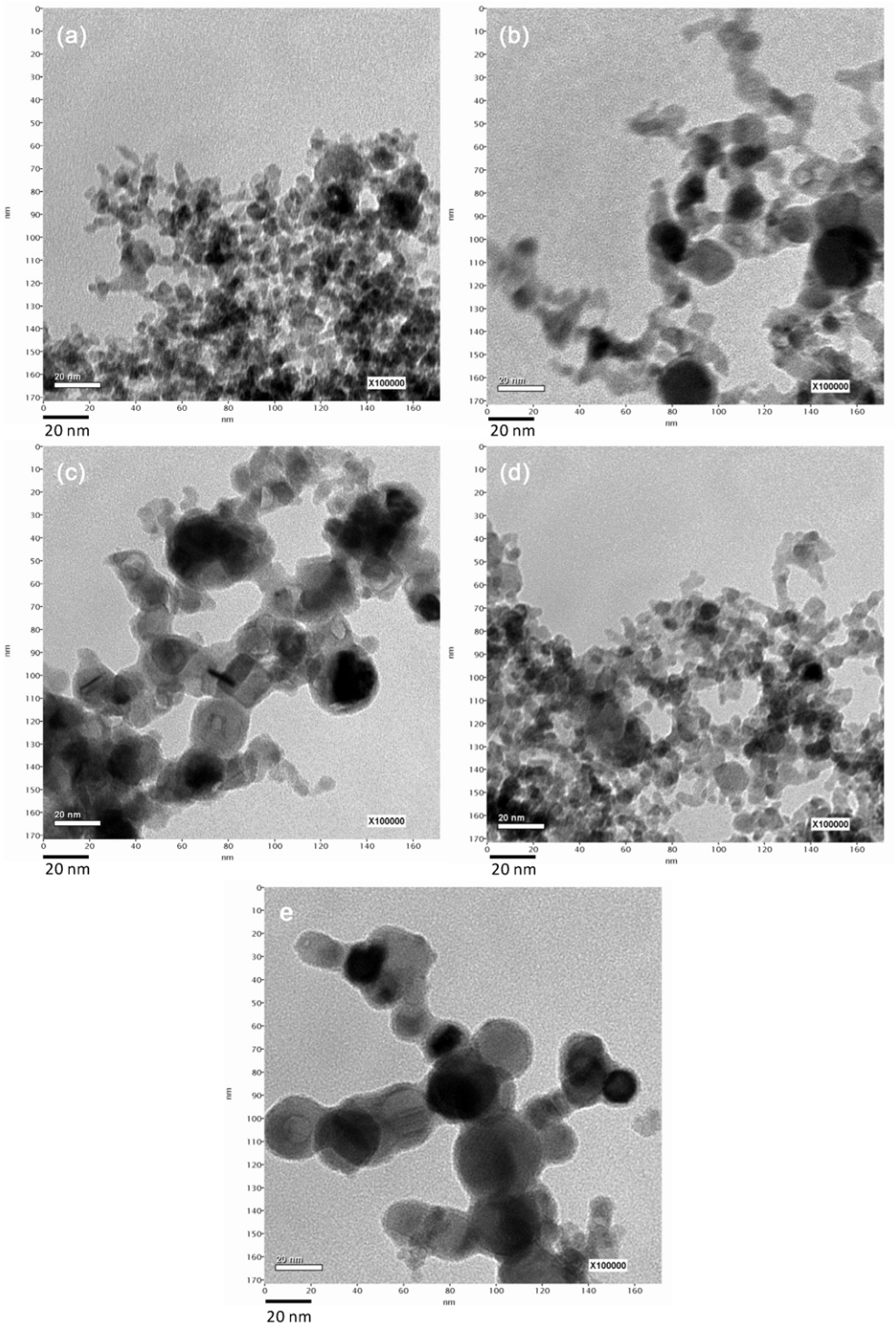

Figure 7. Atmospheric pressure dc glow discharge (0.5 A) between a tungsten rod (∅1.6 mm) and a copper rod (∅9.5 mm) in upward coaxial nitrogen flow. The TEM micrographs correspond to the particle filter samples (*a*) F4, (*b*) F5, (*c*) F6, (*d*) F8 and (*e*) F2 in table 1. The scale bar (20 nm) and the magnification (×100 K) are the same in all the images.

rate of 10 lpm. The reason for this is the higher temperature of the cathode in the experiments at a lower flow rate, resulting in larger cathode erosion rates. From an operational point of view, a minimum gas flow rate is needed to attain a long-term stable continuous source of nanoparticles, depending upon the applied current. Then, the production rate, primary particle size and particle morphology depend in highly nonlinear ways upon the inter-electrode distance and gas flow rate.

4.3. Cathode spot pattern and current density

As can be seen in figure 5, the shape and the texture of the surface of the copper rod change over time under the continuous action of the glow discharge. Figure 8 shows pictures of the cathode surface in the experiments. Figure 8(*a*) corresponds to a fresh copper rod, while the rest of the figures correspond to used copper rods.

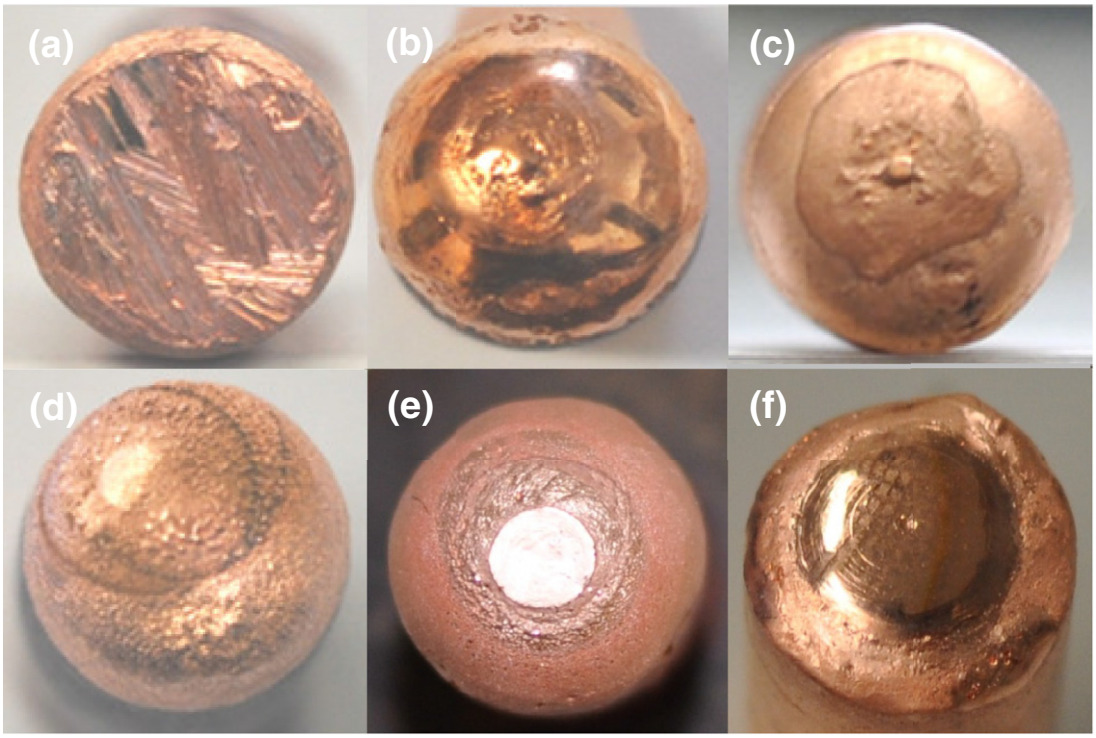

Figure 8. Atmospheric pressure dc glow discharge (0.5 A) between a tungsten rod (∅1.6 mm) and a copper rod (∅9.5 mm) in upward coaxial nitrogen flow. Photographs of (*a*) a fresh copper rod and copper rods used in the experiments: (*b*) gas flow rate of 5 lpm, gap length of 6 mm and duration of 11/2 h; (*c*) gas flow rate of 10 lpm, gap length varying from 1 to 10 mm and duration of 8 h; (*d*) gas flow rate of 10 lpm, gap length of 2 mm and duration of 7 h; (*e*) copper rod (*c*), gas flow rate of 10 lpm, gap length varying from 5 to 13 mm and duration of 3 h; (*f*) gas flow rate of 10 lpm, gap length of 4 mm for 8 h and, then, gap length of 1 mm for 2 h.

Figure 8(*b*) displays the copper rod after the experiment at a gas flow rate of 5 lpm and a gap length of 6 mm shown in figure 4; cavities are observed in the periphery of the frozen rod end. In this experiment a filter collects copper particles before and after cathode melting which are analysed by TEM, with the result shown in figure 9(*a*). Two types of primary particles are distinguished: small nanoparticles (<20 nm) and spherules of sizes ranging from 30 to 100 nm. The former are similar to the nanoparticles displayed in figure 7 and correspond to the period prior to the excursion temperature, when copper is smoothly released from the cathode surface, as depicted in figure 4(*a*). We think larger nanoparticles form after cathode melting, when copper is turbulently released from the bulk molten metal, as can be seen in figures 4(*b*) and (*c*). The large size dispersion of the nanoparticles observed in figure 9(*a*) is due to the spatially inhomogeneous removal rate of copper by the discharge, which continuously moves over the cathode surface. The copper rods in figures 8(*c*)–(*e*) correspond to the experiments at a gas flow rate of 10 lpm. Three concentric regions are distinguished on the cathode surface in figure 8(*c*): a marked small spot (∅ ∼ 0.5 mm) in the centre of a more vague circle (∅ ∼ 2 mm) within a quasi-circular outer region (∅ ∼ 6 mm); the latter corresponds to the region of the cathode surface covered with the negative glow. The cathode pattern in figures 8(*d*) and (*e*) consists of two concentric regions of different textures. The surface of the inner circle (∅ ∼ 2–3 mm) is polished and bright (cathode spot); while the surface of the outer circle (∅ ∼ 6 mm) is bumpy and matte (negative glow). The cathode pattern in figure 8(*f*) includes a central region (∅ ∼ 6–7 mm) with a shiny mirror surface on which many concentric rings are distinguished, surrounded by a harshly eroded region. Also, multiple tiny spots distribute uniformly over the rings. It looks like the cathode spot covers the whole area of the negative glow in the experiment. A TEM micrograph of the copper particles collected onto a filter in this experiment is displayed in figure 9(*b*). Overall they are small nanoparticles like the ones in figure 7, resulting from the erosion of the central region of the cathode surface. In addition, two submicron particles (∼0.2 and 0.8 μm) are observed in figure 9(*b*). Thermal vaporization from a confined thin layer of molten metal (cathode spot) leads to the formation of the nanoclusters and small nanoparticles shown in figure 7. When the cathode heats, the molten layer becomes thicker, extends along the entire cathode surface and eventually bulk melting occurs. Other ablation mechanisms appear which result in larger nanoparticles, submicron- and micron-sized particles like the ones in figures 9(*a*) and (*b*). Then, a metal vapour jet is produced by the cathode surface itself and by a cloud of metal microdroplets released from the cathode surface and evaporating during the flow. The explosive ejection of spherical submicron particles (0.1–1 μm) from the cathode has been commonly observed in atmospheric pressure glow and low current arcs; the phenomenon (cathode jet) has been investigated experimentally [16, 17] and numerically [18–20].

Cathode spot patterns resemble the distribution of the current density over the cathode surface. The variation of the cathode spot area with the inter-electrode distance is not assessed here. Nonetheless, when estimated from the diameter

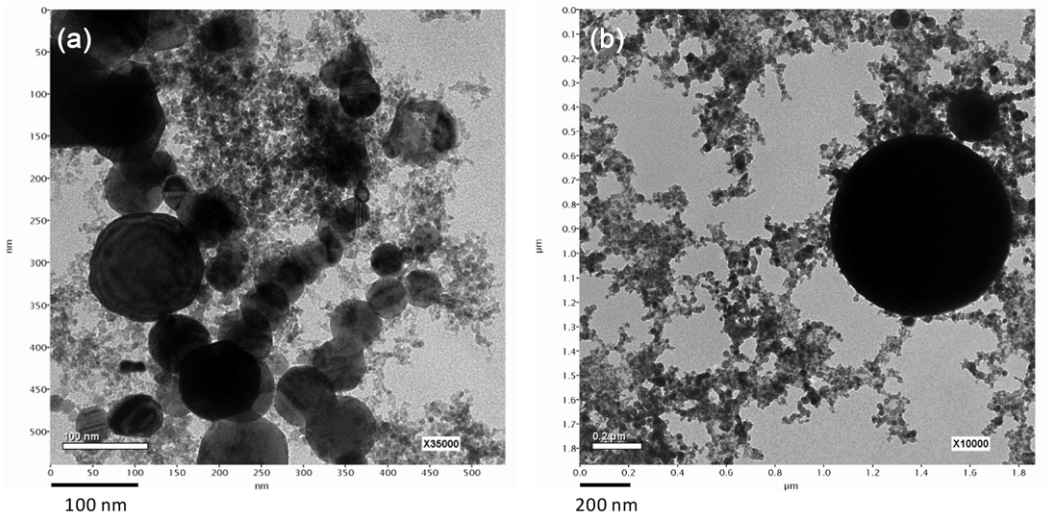

Figure 9. TEM micrographs of copper particles produced by atmospheric pressure dc glow discharge (0.5 A) between a tungsten rod (∅1.6 mm) and a copper rod (∅9.5 mm) in upward coaxial nitrogen flow. The images correspond to the cathode spot patterns in (*a*) figure 8(*b*) and (*b*) figure 8(*f*).

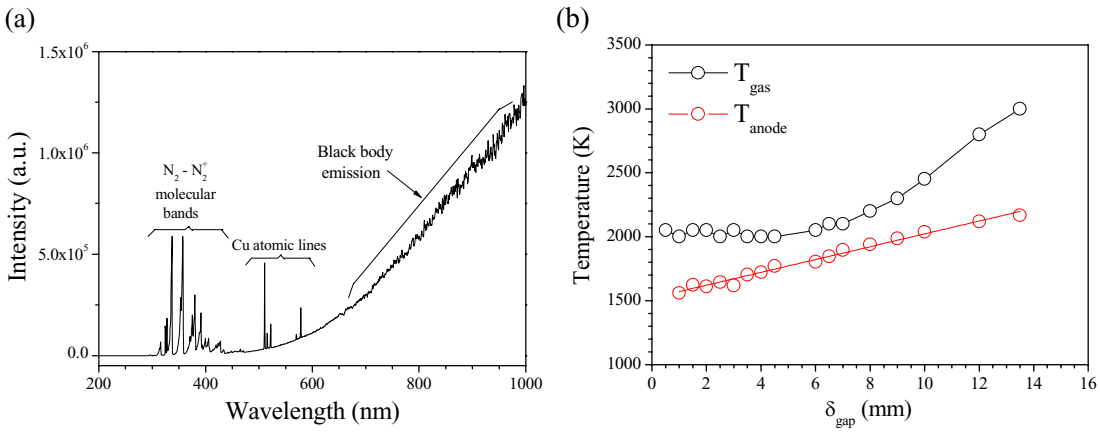

Figure 10. Atmospheric pressure dc glow discharge (0.5 A) between a tungsten rod (∅1.6 mm) and a copper rod (∅9.5 mm) in upward coaxial nitrogen flow (10 lpm). (*a*) Spatially and temporarily integrated emission spectrum correspondent to a gap length of 5 mm. (*b*) Gas temperature and anode temperature versus gap length.

of the cathode spots observed in figures 8(*d*) (∼2 mm) and 8(*f*) (∼6 mm), maximum and minimum values of the current density of 16 and 1.8 A cm^{-2} are obtained. These compare well with the value of 9 A cm^{-2} based on the area of the negative glow reported by Arkhipenko *et al* [9] for atmospheric pressure nitrogen glow discharge between a tungsten rod (∅6 mm) and a hollow copper rod (∅36 mm) with a water cooled surface at the same current of 0.5 A. The variety of cathode spot patterns obtained by glow discharge under the same macroscopic conditions (gap geometry, pressure, glow current, gas flow rate and inter-electrode spacing) are a surprising result of this work. Cathode spot patterns are shown here as relevant to the development and assessment of state of the art numerical models on cathode spot patterns formed in dc glow discharges in gases, like the ones by Almeida *et al* [21–23]. Their model admits multiple multidimensional steady state solutions which are associated with different modes of current transfer to the cathode. These include spotless patterns, axial symmetric patterns like a single spot at the centre and many spots grouped in concentric rings.

4.4. Gas temperature and anode temperature

The light emitted from the glow discharge is monitored by means of a spectrometer in experiments at a current of 0.5 A and a gas flow rate of 10 lpm. Figure 10(*a*) shows the spectrum correspondent to an experiment with a gap length of 5 mm. This is formed of the molecular bands of the second positive system of nitrogen, $N_2(C^3\Pi_u - B^3\Pi_g)$, and the first negative system of the molecular ion, $N_2^+(B^2\Sigma_u^+ - X^2\Sigma_g^+)$, the atomic lines of Cu and a continuous background emission rising toward the infrared range. The latter has the shape of a black body emission and is expected to be produced mostly by the tungsten rod. Although the plasma may have a contribution to the continuous emission, the images in figure 5 show a much brighter and whiter emission from the anode tip. Also, measurements of the glowing anode taken immediately after switching off the discharge show a similar continuous emission profile. The gas temperature is obtained by fitting the measured molecular emission to a simulated N_2 and N_2^+ spectrum for certain values of the rotational and vibrational temperatures.

Table 2. Time averaged discharge voltage and power, width of the positive column and spatially averaged parameters of atmospheric pressure dc glow discharge plasma (0.5 A) between a tungsten rod (∅1.6 mm) and a copper rod (∅9.5 mm) in upward coaxial nitrogen flow (10 lpm) for different values of the inter-electrode gap length.

δ_{gap} (mm)	$V_{voltmeter}$ (V)	P (W)	Column width (mm)	T_{gas} (K)	T_{vib} (K)	T_{exc} (K)	E/N(Td)	N_e (cm^{-3})
1	250	125	—	2000	3000	7500	3.6	—
5	287.5	144	4.5	2000	2800	5800	3.6	3.2×10^{13}
10	360	180	2.7	2450	2900	5300	4.2	7.6×10^{13}
13.5	400	200	2.3	2900	3300	5500	5.2	8.5×10^{13}

The simulations are performed with SPECAIR software [24]. The rotational structure of the measured $N_2(C^3\Pi_u)$ electronic excited level matches that of the molecular ground state, since the excitation takes place by fast electron impact. Also, due to the fast rotational relaxation at atmospheric pressure, it can be assumed that the obtained rotational temperature equals the gas temperature [25]. Due to uncertainties in the fitting process and the low resolution of the spectrometer the error of the gas temperature is about ±100 K. The temperature of the anode is obtained by fitting the continuous emission to that of a black body at a certain temperature. Although most of the black body emission is in the infrared range and hence out of the measuring range, there is still a sufficient emission below 1000 nm to roughly estimate the anode temperature. To that aim, firstly a relative calibration of the spectrometer is carried out with a calibration tungsten ribbon lamp (lamp type P300C) with known emissivity and adjustable temperature. In order to account for deviations from the real emitter (the tungsten rod used in the experiments), the simulated emission of the black body is corrected by the temperature and wavelength dependent tungsten emissivity. The gas temperature and the anode temperature are depicted in dependence of the gap length in figure 10(*b*). It can be seen that the gas temperature stays rather constant at about 2000 K for gap lengths of up to 6 mm and increases with the gap length for larger gaps; at a gap length of 13.5 mm the gas temperature reaches 2900 K. The anode temperature continuously increases with the gap length and remains well below the melting point of tungsten (3695 K). The increase in both the anode temperature and the flow velocity due to gas heating can explain the reduction in the deposition of copper onto the periphery of the tungsten rod with increasing gap length, as observed in the images in figure 5. Also, the tungsten rod with an original length of 0.2 m and linear thermal expansion coefficient of 16.6 K^{-1} enlarges from 1 to 1.5 mm when increasing the temperature from 1500 to 2000 K. Then, the inter-electrode distance reduces with respect to the gap length δ_{gap} set at the beginning of the experiment, as mentioned in section 4.

4.5. Plasma parameters

Table 2 shows a set of measured and calculated parameters of the glow discharge for several values of the gap length. As explained above, the spectroscopic measurements are taken with no spatial resolution, what means the results are representative of the largest and brightest section of the glow discharge, the positive column. The vibrational temperature represents that of some vibrational levels within $N_2(C^3\Pi_u)$. It must be taken only as an approximation, since different electronic excitation and heavy particle relaxation processes can take place for different electronic and vibrational levels. In particular, we use the bands correspondent to vibrational transitions 0–1, 1–2 and 2–3 with band heads at 357.6, 353.6 and 350.0 nm. The excitation temperature is obtained with a Boltzman plot of the measured Cu lines. The temperatures satisfy the inequality $T_{gas} < T_{vib} < T_{exc}$. The excited atomic Cu levels are produced by electron collisions and consequently the values of T_{exc} are close to the high electron temperature (about 1 eV in N_2 atmospheric pressure glow discharges) [9], although below it due to the loss of excited atoms by radiation and ionization. Similarly, vibrational levels of N_2 are produced by inelastic collisions with electrons and other gas molecules and consequently the values of T_{vib} are between the gas temperature and the excitation temperature. Due to high efficiency of the inelastic collisions between N_2 molecules that exchange vibrational kinetic energy [35], the values of T_{gas} and T_{vib} are closer to each other while T_{exc} remains higher and closer to the electron temperature. In non-thermal plasmas it is expected that the temperature of the electrons is much higher than the gas temperature [9], as observed in table 2. It can also be seen that the power and the electron density rise with the gap length and, then, the three temperatures come closer. This indicates that the discharge is evolving towards a thermal arc discharge, as was observed in [9, 10, 15]. However, the three temperatures are not equal yet and the structure and the voltage of the discharge are still those of a glow discharge. The reduced electric field E/N is derived from the gas temperature and the electric field strength shown in figures 10(*b*) and 2(*b*), respectively. An estimation of the electron density N_e is calculated with the Ohm's law and the values of the reduced electric field and current density in the positive column. The values of the reduced electric field and the electron density in table 2 compare well with those reported by Arkhipenko *et al* [13]. Finally, from the photographs of the glow discharge it is possible to estimate the width of the positive column. It is found that the column contracts rapidly for larger gaps ($\delta_{gap} > 6$ mm), as observed also in figure 5.

5. Discussion

At the high current densities attained in the experiments volumetric gas heat generation occurs in the cathode fall. The heat volume source is commonly estimated as the product of the current density and the electric field in the cathode fall, and the cathode fall voltage is obtained by extrapolating the discharge voltage-gap length characteristic down to zero gap. A value

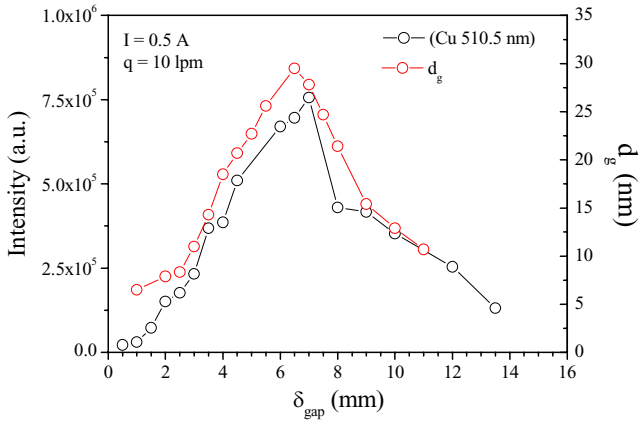

Figure 11. Atmospheric pressure dc glow discharge (0.5 A) between a tungsten rod (∅1.6 mm) and a copper rod (∅9.5 mm) in upward coaxial nitrogen flow (10 lpm). Intensity of the atomic line of Cu of 510.5 nm (emission spectrometry) and geometric mean diameter of the copper nanoparticles (SMPS) versus gap length.

of nearly 250 V is obtained from the curve in figure 2(*b*) for the cathode fall voltage in the experiments at a current of 0.5 A and a gas flow rate of 10 lpm. The height of the cathode fall is unknown and, thus, we assume a value of 70 μm, as reported by Arkhipenko *et al* [9]. Then, we obtain a rough estimate of 35 kV cm^{-1} for the electric field in the cathode fall and values of the heat volume source from 63 to 560 kW cm^{-3}. The latter leads to intense gas heating and, consequently, to cathode heating. This is also due to the bombardment of the cathode surface by ions launched from the plasma and accelerated in the strong electric field in the cathode fall and by fast neutral molecules created in collisions with ions in the cathode fall. The cathode temperature has a significant influence on the properties of the cathode fall [26–31] and on the cathode vaporization rate. In addition, the vaporization rate and the gas temperature determine the saturation state of the vapour in the gas which in turn determines the concentration and size of the primary particles. Therefore, the cathode temperature is a key control parameter when using atmospheric pressure glow discharge to evaporate the cathode material for nanoparticle production [32].

The cathode temperature is not measured in this work. The intensity of the atomic line of Cu of 510.5 nm in wavelength and the geometric mean diameter of the size distribution of copper particles shown in figure 6(*a*) are depicted in dependence of the gap length in figure 11. The good correlation between the two curves is noticed along with the mass production rate in table 1; hence also the correlation between the cathode vaporization rate and nanoparticle production. Thus, the same dependence on the gap length is inferred for the cathode temperature which differs, however, from the gap length dependence of the gas temperature displayed in figure 10(*b*). It is noticed that the latter represents the spatial average of the gas temperature over the plasma volume to which the positive column contributes the most, whereas the cathode temperature follows the temperature of the gas in the cathode fall. This may be significantly lower, from several hundred to several thousand degrees depending upon current and cathode cooling, than the gas temperature in the positive column [9, 13, 26]. Nonetheless, an abrupt change in the tendency both of the gas temperature and the cathode evaporation rate is observed in figure 10(*b*) and figure 11, respectively, at a gap length of nearly 6 mm. Beyond 6 mm, the gas temperature increases while the cathode vaporization rate diminishes with increasing gap length. In addition, the glow discharge continuously contracts for gap lengths larger than 6 mm. Therefore, one could think that the three features are related to each other. This issue is not further investigated here, since it requires spatially resolved spectrometric measurements that discern between the positive column and the cathode fall. In particular, measuring the temperatures, the metal vapour concentration and the electron density in the cathode fall is of great importance. In this region, the main ionization takes places to sustain the discharge and it is also where the metal vapour is released into the gas.

Some potential explanations for the behaviour of large glow discharges observed in the experiments are given in the following. At high currents atmospheric pressure dc glow discharge is usually accompanied by transient arc discharges [7]. Ding *et al* [33] investigated the effect of the inter-electrode spacing on the stability of an atmospheric pressure air dc glow discharge sustained by a resonant power supply in a pin-to-plate configuration. They found that arcing disappears for values of the gap length larger than 4 mm, when the capacitance of the inte-electrode gap becomes less than the intrinsic impedance of the power supply. That could explain the reduction in the cathode vaporization rate for gap lengths larger than 6 mm. Also, the vibration to translational (VT) relaxation of the nitrogen molecules may be responsible for gas heating in the positive column of glow discharges. If the residence time of the flow in the discharge column is long enough to attain the VT transfer, the gas is heated [34]. In our experiments the velocity of the nitrogen flow in the inter-electrode gap at a temperature of 2000 K is roughly of 10 m s^{-1}, resulting in a residence time of 6×10^{-4} s for a gap of 6 mm in length. This value compares well with experimental values of the VT relaxation time for nitrogen reported in the literature [35, 36].

6. Conclusions

This work proves that it is feasible to attain continuous stable source of nanoparticles by atmospheric pressure dc glow discharge between two electrodes in upward coaxial inert gas flow, as long as cathode melting is prevented. This is attained by a suitable election of the cathode size and the gas flow rate depending upon the discharge current. This work provides also insight and guidance into the use of the gas flow rate and the inter-electrode distance as to adjust the production rate and primary particle size of the nanoparticles. The latter are complex nonlinear functions of the two process parameters. These need to be tuned up to produce the best quality nanoparticles at the highest attainable yield for a given application. At a current of 0.5 A and a nitrogen flow rate of 10 lpm copper nanoparticles have been produced at a yield from 1 to 10 mg h^{-1} when increasing the electrical power from 125 to 137.5 W by enlarging the inter-electrode distance from 0.5 to 5 mm. Also, the primary particle size

increases from roughly 8 nm to nearly 20 nm. Beyond 5 mm, the discharge power continues to rise whereas nanoparticle production diminishes with increasing inter-electrode distance. This feature needs to be further investigated in the light of the changes in the structure and properties of the glow discharge observed in this work. It is found that optical emission spectrometry is an affordable technique suitable for monitoring and controlling nanoparticle production by vaporization of a cathode by means of electrical discharges. Cathode ablation modes other than thermal surface vaporization may appear during atmospheric pressure glow discharge, which have significant implications both for particle yield and particle size. Finally, spatially resolved spectrometric measurements will be conducted dependent of the inter-electrode distance in a future work. These will allow to discern plasma properties in the positive column and in the cathode fall and to correlate them with nanoparticle production.

Acknowledgments

This research work has been financially supported by the European Union's Seventh Framework Program (EU FP7) under Grant Agreement No. 280765 (BUONAPART-E).

References

[1] Kruis F E, Stein M and Hontañón E 2013 *Proc. AIChE Annual Meeting (San Francisco, CA, November 2013)* http://www3.aiche.org/proceedings/Abstract.aspx?PaperID=316777
[2] Pfeiffer T V, Feng J and Schmidt-Ott A 2014 *Adv. Powder Technol.* **25** 56–70
[3] Stein M, Kiesler D and Kruis F E 2013 *J. Nanopart. Res.* **15** 1400
[4] Stein M, Kiesler D and Kruis F E 2013 *Aerosol Sci. Technol.* **47** 1276–84
[5] Boyle W S and Haworth F E 1956 *Phys. Rev.* **101** 935–8
[6] Fan H Y 1939 *Phys. Rev.* **55** 769–75
[7] Hontañón E, Palomares J M, Stein M, Guo X, Engeln R, Nirschl H and Kruis F E 2013 *J. Nanopart. Res.* **15** 1957
[8] Sreenivas A and Karady G G 1991 *Proc. IEEE Particle Accelerator Conf. (San Francisco, CA, May 1991)* pp 949–51 http://ieeexplore.ieee.org/stamp/stamp.jsp?tp=&arnumber=164500
[9] Arkhipenko V I, Kirillov A A, Safronau Y A, Simonchik L V and Zgirouski S M 2012 *Eur. Phys. J.* D **66** 252
[10] Staack D, Farouk B, Gutson A and Fridman A 2005 *Plasma Sources Sci. Technol.* **14** 700–11
[11] Gambling W A and Edels H 1954 *Br. J. Appl. Phys.* **5** 36–9
[12] Simonchik L, Pitchford L and Safronau Y 2012 *Proc. 20th Europhysics Conf. on the Atomic and Molecular Physics of Ionizes Gases ESCAMPIG (Viana do Costelo, Portugal, July 2012)* http://escampig2012.ist.utl.pt/Proceedings/files/Topic%2010/escampig2012_submission_217.pdf
[13] Arkhipenko V I, Kirillov A A, Safronau Ya A, Simonchik L V and Zgirouski S M 2008 *Plasma Sources Sci. Technol.* **17** 045017
[14] Xuechen L I, Huanhuan Z and Pengying J I A 2013 *Plasma Sci. Technol.* **15** 1149–53
[15] Machala Z, Marode E, Laux C O and Kruger C H 2004 *J. Adv. Oxid. Technol.* **7** 133–7
[16] Jeanvoine N 2009 Plasma-material interaction and electrode degradation in high voltage ignition discharges *PhD Thesis* (University of Saarbrücken, Germany) http://d-nb.info/100015940X/34
[17] Gray E W and Pharney J R 1974 *J. Appl. Phys.* **45** 667–71
[18] Soldera F, Lasagni A, Mücklich F, Kaiser T and Hrastnik K 2005 *Comput. Mater. Sci.* **32** 123–39
[19] Vasenin Y 2002 *Proc. 20th Int. Symp. on Discharges and Electrical Insulation in Vacuum (Tours, France, June–July 2002)* doi.org/10.1109/ISDEIV.2002.1027393
[20] Llewellyn-Jones F 1966 *The Glow Discharge: and an Introduction to Plasma Physics (London: Methuen & Co.)*
[21] Almeida P G C and Benilov M S 2013 *Phys. Plasmas* **20** 101613
[22] Almeida P G C, Benilov M S and Faria M J 2011 *IEEE Trans. Plasma Sci.* **39** 2190–1
[23] Almeida P G C, Benilov M S and Faria M J 2010 *Plasma Sources Sci. Technol.* **19** 025019
[24] Laux C O, Gessman R J, Kruger C H, Roux F, Michaud F and Davis S P 2001 *J. Quant. Spectrosc. Radiat.* **68** 473–82
[25] Laux C O, Spence T G, Kruger C H and Zare R N 2003 *Plasma Sources Sci. Technol.* **12** 125–38
[26] Arkhipenko V I, Kirillov A A, Safronau Ya A, Simonchik L V and Zgirouski S M 2008 *Plasma Sources Sci. Technol.* **18** 045013
[27] Winter J, Lange H and Golubovskii Yu B 2008 *J. Phys. D: Appl. Phys.* **41** 085201
[28] Arkhipenko V I, Kirillov A A, Simonchik L V and Zgirouski S M 2007 *Publ. Astron. Obs. Belgrade* **82** 11–21
[29] Arkhipenko V I, Zgirovskii S M, Kirillov A A and Simonchik L V 2002 *Plasma Phys. Rep.* **28** 858–65
[30] Shi J J and Kong M G 2003 *J. Appl. Phys.* **94** 5504–13
[31] Arslanbekov R R 2000 *J. Phys. D: Appl. Phys.* **33** 524–44
[32] Boagerts A and Gibjels R 2004 *J. Anal. At. Spectrom.* **19** 1206–12
[33] Ding W, Li F and Yang L 2009 *IEEE Trans. Plasma Sci.* **37** 2207–12
[34] Machala Z, Laux C O, Duten X, Packan D M, Yu L and Kruger C H 2003 *Proc. 41st Aerospace Sciences Meeting and Exhibit (Reno, NV, January)* Paper 874
[35] Sebacher D J 1967 *AIAA J.* **5** 819–20
[36] Lukasik S J and Young J E 1957 *J. Chem. Phys.* **27** 1149–55